



# Theory of local dynamical magnetic susceptibilities from the Korringa-Kohn-Rostoker Green function method

S. Lounis,<sup>1,\*</sup> A. T. Costa,<sup>1,2</sup> R. B. Muniz,<sup>2</sup> and D. L. Mills<sup>1</sup>

<sup>1</sup>*Department of Physics and Astronomy, University of California Irvine, California 92697, USA*

<sup>2</sup>*Instituto de Física, Universidade Federal Fluminense, Niterói, Rio de Janeiro 24210-340, Brazil*

(Received 6 October 2010; published 13 January 2011)

Within the framework of time-dependent density functional theory combined with the Korringa-Kohn-Rostoker Green function formalism, we present a real-space methodology to investigate dynamical magnetic excitations from first principles. We set forth a scheme which enables one to deduce the correct effective Coulomb potential needed to preserve the spin-invariance signature in the dynamical susceptibilities, that is, the Goldstone mode. We use our approach to explore the spin dynamics of  $3d$  adatoms and different dimers deposited on a Cu(001) with emphasis on their decay to particle-hole pairs.

DOI: [10.1103/PhysRevB.83.035109](https://doi.org/10.1103/PhysRevB.83.035109)

PACS number(s): 75.75.-c, 71.15.-m, 75.30.Hx, 75.40.Gb

## I. INTRODUCTION

The magnetic functionalization of nanostructures made of few atoms requires the understanding of spin excitations at the nanoscale and subnanoscale levels. Recently, state-of-the-art experiments based on scanning tunneling microscopy (STM) were utilized to excite and control the magnetic states of single adatoms sitting on semi-insulating<sup>1</sup> or metallic<sup>2,3</sup> surfaces. The spin dynamics of moment-bearing  $3d$  metal atoms have been probed in those experiments but often the theoretical picture used for the interpretation is based on a model Hamiltonian describing an atomlike localized moment with integer or half-integer spin. Such a model is useful only for systems where the substrate interacts weakly with the adsorbate;<sup>1</sup> it fails qualitatively to describe cases with strong coupling to the substrate electrons where hybridization leads to moments far from integer and half-integer values and  $d$  levels with widths that can range from a few hundred millivolts to perhaps an electron volt. This paper presents a scheme wherein one may address the commonly encountered strongly coupled systems, with density-functional theory as the basis. In contrast to empirical tight-binding schemes used earlier,<sup>4-7</sup> the method set forth in this paper incorporates a proper *ab initio*-based description of the one-electron physics from upon which our description of spin dynamics is erected. Also the scheme set forth in this paper may be implemented with modest computational labor.

Several approaches have been proposed to describe inelastic STM experiments involving the aforementioned local moment picture,<sup>8-12</sup> but none are based on taking full account of the electronic structure of the adsorbates as well as the substrates including the effects of hybridization. The latter requires, among other ingredients,<sup>13</sup> the evaluation of the transverse magnetic response function  $\chi$  or the so-called transverse dynamical magnetic susceptibility that relates, in linear-response theory, the amplitude of the transverse spin motion  $m_{x,y}$  produced by a transverse external magnetic field  $B_{\text{ext}}$  of frequency  $\omega$ . There are three major roads followed to compute  $\chi$ : (i) empirical tight-binding (ETB) theory,<sup>4-7</sup> (ii) time-dependent density-functional theory (TD-DFT),<sup>14-21</sup> and (iii) many-body perturbation theory (MBPT) using the random-phase approximation (RPA) and DFT.<sup>22,23</sup> The calculation of  $\chi$  requires one to solve a Dyson

equation whose solution may be written schematically in the form

$$\chi = \chi_0(1 - U\chi_0)^{-1}. \quad (1)$$

As noted in Ref. 21,  $\chi_0$  is described by a different nomenclature depending on the method used to calculate it. Within TD-DFT,<sup>14,15</sup>  $\chi_0$  is known as the Kohn-Sham susceptibility and  $U$  is the exchange and correlation kernel that, if ideally known completely, would render Eq. (1) the exact solution.  $U$  is obviously approximated in practice, for example, by the adiabatic local spin-density approximation. It turns out that evaluating Eq. (1) is computationally very challenging, especially within the TD-DFT or the MBPT. This explains the very few calculations found in the literature, almost all of which address bulk systems. This makes it even more challenging to simulate inelastic STM experiments that examine adatoms deposited on surfaces. Recently, we developed a method<sup>21</sup> that handles the calculation of the transverse dynamical magnetic susceptibility in a scheme that resembles ETB but is based on TD-DFT. Thus, the method incorporates full self-consistent first-principles calculations of the underlying electronic structure. Two interesting results were obtained: (i) A justification of the Lowde and Windsor scheme<sup>24</sup> emerged from the analysis and (ii) values of  $U$  determined from first principles for different systems are in accordance with the empirical values extracted from photoemission data by Himpsel.<sup>25</sup>

In our previous paper,<sup>21</sup> we addressed a central question related to the practical determination of  $\chi_0$  and  $U$ , within the framework of density-functional-based schemes. It is known, but often not discussed explicitly, that the Goldstone theorem is not satisfied, in practice, when solving Eq. (1) within TD-DFT schemes. We remark that within the framework of the ETB scheme, the Goldstone theorem is satisfied exactly, as demonstrated earlier.<sup>6</sup> The Goldstone theorem, when satisfied, ensures that the zero-wave-vector spin waves have precisely zero frequency (when spin-orbit coupling is set aside). The reason the Goldstone theorem is not satisfied within density-functional-based schemes is that the numerical methods used to extract  $U$  and  $\chi_0$  are not compatible with the Ward identity. To compensate for this problem, Sasioglu *et al.*<sup>23</sup> correct  $U$  by 45% in their study of bulk Ni, while Buczek *et al.* find

a finite frequency for the Goldstone mode.<sup>19</sup> To cure such inconsistencies, an *ad hoc* shift by hand of the value of  $U$  is used commonly. Our aim is to demonstrate that such corrections could be dangerous, for instance, when the system under investigation contains more than two atoms in the unit cell. In Ref. 21, we set forth and utilized a sum rule that allows one to generate a  $U$  that is fully compatible with the Goldstone mode.

The discussion of the sum rule in Ref. 21 was brief, though its application was illustrated. In this paper, we provide a detailed derivation of our scheme,<sup>21</sup> including the sum rule needed to determine  $U$ . Our method is based on the Korringa-Kohn-Rostoker single-particle Green function (KKR-GF),<sup>26</sup> which contains an *ab initio* description of the electronic structure.

We remark that in earlier work, the ETB method has been used successfully to describe spin waves in films on substrates<sup>5,7</sup> along with the spin dynamics of adatoms as probed in the recent STM experiments.<sup>6</sup> In this approach, it is necessary to make contact with electronic structure calculations for the purpose of extracting the tight-binding parameters required to describe the one-electron properties of the system of interest. Often appropriate electronic structure calculations are unavailable, or if they are it can be a challenge to extract appropriate parameters in an unambiguous manner for complex systems such as ultrathin films adsorbed on substrates. The approach we develop here eliminates this issue completely, while at the same time it provides a computationally straightforward scheme for generating the dynamic transverse susceptibility.

## II. STRUCTURE OF THE THEORY: THE SUM RULE AND THE EFFECTIVE $U$

It is, of course, possible in principle to calculate the Kohn-Sham noninteracting susceptibility  $\chi_0$ . In this section, we show that once  $\chi_0$  is assumed to be known, we can derive a prescription for generating the effective Coulomb interaction  $U$  which enters Eq. (1) that is fully compatible with the Goldstone theorem. In effect,  $U$  is a functional of  $\chi_0$ . With  $U$  determined in the manner we describe, there is no reason for *ad hoc* adjustment of this central parameter. We also describe a scheme which allows one to generate a physically sensible approximation to  $\chi_0$  that is straightforward and simple to implement. We then use this scheme to generate a series of explicit predictions regarding the nature of spin excitations of adatoms and adatom dimers.

To begin, we assume we have in hand a magnetic system with an initial charge density  $n_0(\vec{r})$ . Its ground-state magnetization  $[m_z(\vec{r})]$  pointing along, say, the  $z$  direction experiences a modification induced by a small time-dependent external transverse magnetic field  $B_{\text{ext}}(\vec{r}; t)$ . The result is an induced transverse magnetization  $m_{x,y}(\vec{r}; t)$  localized in the  $(xy)$  plane perpendicular to the direction  $z$ . To describe the transverse magnetization, we begin by calculating the frequency-dependent Kohn-Sham transverse susceptibility, or  $\chi_0$ , which may be expressed in the form

$$\chi_0^{ij}(\vec{r}, \vec{r}'; \omega) = -\frac{1}{\pi} \int dz f(z) [G_{ij}^{\downarrow}(\vec{r}, \vec{r}'; z + \omega) \text{Im} G_{ji}^{\uparrow}(\vec{r}', \vec{r}; z) + \text{Im} G_{ij}^{\downarrow}(\vec{r}, \vec{r}'; z) G_{ji}^{\uparrow}(\vec{r}', \vec{r}; z - \omega)], \quad (2)$$

where  $f(z)$  is the Fermi distribution function,  $G$  and  $G^-$  represent the retarded and advanced one particle Green functions connecting atomic sites  $i$  and  $j$ , respectively, and  $\text{Im} G = -\frac{i}{2}(G - G^-)$ .

A comment on the notation is in order. In general, the point  $\vec{r}$  is in unit cell  $i$ , and  $\vec{r}'$  is in unit cell  $j$ . These vectors are measured from the center of their respective unit cells. Thus, if we wish to describe these two points with respect to a master origin  $O$ , we describe the notation  $\vec{r} + \vec{R}_i$  and  $\vec{r}' + \vec{R}_j$ , respectively, where  $\vec{R}_{i,j}$  are vectors from  $O$  to the center points of cell  $i, j$ . With this convention in mind, the single-particle Green function, often described as  $G(\vec{r} + \vec{R}_i, \vec{r}' + \vec{R}_j, z)$ , will here be described as  $G_{ij}(\vec{r}, \vec{r}'; z)$ , a notation that is very convenient when the KKR scheme we employ is utilized.

To derive our criterion for choosing an effective  $U$ , our interest is in the static form of the Kohn-Sham susceptibility. At  $\omega = 0$ , the expression in Eq. (2) reduces to the usual form of the static magnetic susceptibility:

$$\chi_0^{ij}(\vec{r}, \vec{r}'; 0) = \frac{i}{2\pi} \int dz f(z) [G_{ij}^{\downarrow}(\vec{r}, \vec{r}'; z) G_{ji}^{\uparrow}(\vec{r}', \vec{r}; z) - G_{ij}^{\downarrow}(\vec{r}, \vec{r}'; z) G_{ji}^{\uparrow}(\vec{r}', \vec{r}; z)]. \quad (3)$$

Our first step is to multiply both sides of Eq. (3) by  $B_{\text{eff}}^j(\vec{r}'; \omega = 0)$  and then we integrate over  $\vec{r}'$  within the atomic site  $j$  and sum up over all sites  $j$ :

$$\sum_j \int d\vec{r}' \chi_0^{ij}(\vec{r}, \vec{r}'; 0) B_{\text{eff}}^j(\vec{r}'; 0) = \frac{i}{2\pi} \int dz f(z) \sum_j \int d\vec{r}' [G_{ij}^{\downarrow}(\vec{r}, \vec{r}'; z) B_{\text{eff}}^j(\vec{r}'; 0) G_{ji}^{\uparrow}(\vec{r}', \vec{r}; z) - G_{ij}^{\downarrow}(\vec{r}, \vec{r}'; z) B_{\text{eff}}^j(\vec{r}'; 0) G_{ji}^{\uparrow}(\vec{r}', \vec{r}; z)]. \quad (4)$$

$B_{\text{eff}}$  is given by the difference between the potentials of each spin channel ( $V_{\downarrow} - V_{\uparrow}$ ).

We next use an identity derived in the Appendix that relates the Green function for a given spin channel, say  $\uparrow$ , to the Green function of the opposite spin channel through the potential difference  $B_{\text{eff}}$ :

$$G_{ii}^{\uparrow}(\vec{r}, \vec{r}; z) = G_{ii}^{\downarrow}(\vec{r}, \vec{r}; z) + \sum_j \int d\vec{r}' G_{ij}^{\downarrow}(\vec{r}, \vec{r}'; z) B_{\text{eff}}^j(\vec{r}'; 0) G_{ji}^{\uparrow}(\vec{r}', \vec{r}; z) \quad (6)$$

or

$$G_{ii}^{\uparrow}(\vec{r}, \vec{r}; z) - G_{ii}^{\downarrow}(\vec{r}, \vec{r}; z) = \sum_j \int d\vec{r}' G_{ij}^{\downarrow}(\vec{r}, \vec{r}'; z) B_{\text{eff}}^j(\vec{r}'; 0) G_{ji}^{\uparrow}(\vec{r}', \vec{r}; z). \quad (7)$$

Similar relations but written differently have been already used for example in Refs. 27 and 6.

Thus, Eq. (5) becomes

$$\sum_j \int d\vec{r}' \chi_0^{ij}(\vec{r}, \vec{r}'; 0) B_{\text{eff}}^j(\vec{r}'; 0) = \frac{i}{2\pi} \int dz f(z) [G_{ii}^{\uparrow}(\vec{r}, \vec{r}; z) - G_{ii}^{\downarrow}(\vec{r}, \vec{r}; z) - G_{ii}^{\downarrow}(\vec{r}, \vec{r}; z) + G_{ii}^{\uparrow}(\vec{r}, \vec{r}; z)], \quad (8)$$

which is the same as

$$\sum_j \int d\vec{r}' \chi_0^{ij}(\vec{r}, \vec{r}'; 0) B_{\text{eff}}^j(\vec{r}'; 0) = -\frac{1}{\pi} \int dz f(z) \times [\text{Im} G_{ii}^{\uparrow}(\vec{r}, \vec{r}; z) - \text{Im} G_{ii}^{\downarrow}(\vec{r}, \vec{r}; z)]. \quad (9)$$

One can recognize that the right-hand side of the previous equation is simply  $m_z^i(\vec{r}; 0)$ . Thus, we obtain the final form of an important sum rule:

$$\sum_j \int d\vec{r}' \chi_0^{ij}(\vec{r}, \vec{r}'; \omega = 0) B_{\text{eff}}^j(\vec{r}'; \omega = 0) = m_z^i(\vec{r}; \omega = 0). \quad (10)$$

We remark that within the ETB scheme, a statement equivalent to Eq. (10) is found in Ref. 6.

The Kohn-Sham susceptibility  $\chi_0^{ij}(\vec{r}t, \vec{r}'t')$  can be expanded in terms of real spherical harmonics,  $Y$ , and when this is done it can be expressed as a sum over angular momenta  $L, L_1, L_2$ , and  $L_3$  as  $\sum_{LL_1L_2L_3} \chi_0^{iLL_1; jL_2L_3}(rt, r't') Y_L(\hat{r}) Y_{L_1}(\hat{r}') Y_{L_2}(\hat{r}') Y_{L_3}(\hat{r}')$ . This follows since  $\chi_0$  is a convolution of single-particle Green functions [see Eq. (2)]. Consequently, within the atomic sphere approximation (ASA) and assuming a spherical magnetic field  $m_{x,y}^i(\vec{r}t) = m_{x,y}^i(rt)$ ,  $m_z^i(\vec{r}t) = m_z^i(rt)$  and  $B_{\text{ext}}^j(\vec{r}'t) = B_{\text{ext}}^j(r't)$ , Eq. (10) reads

$$\sum_j \int d\vec{r}' \sum_{LL_1L_2L_3} Y_L(\hat{r}) Y_{L_3}(\hat{r}) \chi_0^{iLL_1; jL_2L_3}(r, r'; 0) B_{\text{eff}}^j(r'; 0) \times \int d\hat{r}' Y_{L_1}(\hat{r}') Y_{L_2}(\hat{r}') = m_z^i(r; 0). \quad (11)$$

If one integrates both sides of the previous equation over  $d\hat{r}$  and uses  $\int d\hat{r} Y_L(\hat{r}) Y_{L'}(\hat{r}) = \delta_{LL'}$ , one finds

$$\sum_j \int d\vec{r}' \sum_{LL_1} \chi_0^{iLL_1; jL_1L}(\vec{r}, \vec{r}'; 0) B_{\text{eff}}^j(\vec{r}'; 0) = 4\pi m_z^i(r; 0). \quad (12)$$

If we define

$$U^j(r') = \frac{B_{\text{eff}}^j(r'; 0)}{4\pi m_z^j(r'; 0)}, \quad (13)$$

that is the usual form for the effective  $U$  that enters Eq. (1) as generated from the adiabatic local spin density approximation (ALDA) given in the upcoming section, then Eq. (12) can be rewritten as

$$\sum_j \int d\vec{r}' \sum_{LL_1} \chi_0^{iLL_1; jL_1L}(\vec{r}, \vec{r}'; 0) m_z^j(r'; 0) U^j(r') = m_z^i(r; 0) \quad (14)$$

or as

$$\sum_j \int d\vec{r}' \Gamma^{ij}(\vec{r}, \vec{r}') U^j(r') = m_z^i(r; 0), \quad (15)$$

with  $\Gamma^{ij}(\vec{r}, \vec{r}') = \sum_{LL_1} \chi_0^{iLL_1; jL_1L}(\vec{r}, \vec{r}'; 0) m_z^j(r'; 0)$ .

In matrix notation, Eq. (15) can be expressed as

$$\Gamma \vec{U} = \vec{m}_z, \quad (16)$$

which provides a means of calculating of  $U$ :

$$\vec{U} = \Gamma^{-1} \vec{m}_z. \quad (17)$$

Equation (17) allows us to generate  $U$  through knowledge of only the ground-state magnetization and the Kohn-Sham susceptibility  $\chi_0$ . An analysis of Eq. (1) shows that in the absence of an external magnetic field parallel to the  $z$  direction the full dynamic susceptibility  $\chi$  will have a pole at zero frequency, if in fact  $U$  is generated from Eq. (17). Thus, by this scheme we generate an effective  $U$  compatible with the Goldstone theorem. Stated otherwise, the correct  $U$  is the one with the lowest eigenvalue of the denominator of Eq. (1) associated with the magnetic moments as components of the eigenvectors. In the following we show through explicit calculation that the prescription in Eq. (17) can be applied to clusters of moment-bearing ions which consist of dissimilar atoms.

### III. THE MASTER DYSON EQUATION WITHIN TD-DFT

Let us briefly derive the master Dyson equation which leads to Eq. (1) within the TD-DFT. By applying a linear variational approach, one assumes similar initial conditions as the ones in the previous section, that is, a magnetic system with an initial charge density  $n_0(\vec{r})$ , a magnetization pointing along the  $z$  direction, and an exciting time-dependent transverse magnetic field  $B_{\text{ext}}(\vec{r}; t)$  with small magnitude that allows us to use linear-response theory. The result is an induced transverse magnetization localized in the  $(xy)$  plane perpendicular to the direction  $z$ . The art of TD-DFT is to relate and connect the induced transverse magnetization  $m_{x,y}(\vec{r}; t)$  to the externally applied magnetic field. The dynamic susceptibility we seek may be expressed as a functional derivative of the transverse moment with respect to the external field, evaluated at zero external field,

$$\chi^{ij}(\vec{r}t, \vec{r}'t') = \left. \frac{\delta m_{x,y}^i[B_{\text{ext}}](\vec{r}t)}{\delta B_{\text{ext}}^j(\vec{r}'t')} \right|_{B_{\text{ext}}=0, n_0}, \quad (18)$$

where  $\chi$  is the response function we seek. In regard to the superscripts  $i, j$  and the definition of the vectors  $\vec{r}, \vec{r}'$ , see the remarks after Eq. (2). The convention we use here is the same as that employed for the single-particle Green function.

Within the ASA and assuming once more an applied magnetic field with spherical symmetry within the unit cell, we may write

$$m_{x,y}^i(\vec{r}t) = \sum_j \int d\vec{r}' \int dt' \chi^{ij}(\vec{r}t, \vec{r}'t') B_{\text{ext}}^j(\vec{r}'t'). \quad (19)$$

Upon resorting to the spherical harmonic expansion discussed earlier, this becomes

$$m_{x,y}^i(rt) = \sum_j \int d\vec{r}' \int dt' \sum_{LL_1L_2L_3} \chi^{iLL_1; jL_2L_3}(rt, r't') \times Y_L(\hat{r}) Y_{L_1}(\hat{r}') Y_{L_2}(\hat{r}') Y_{L_3}(\hat{r}') B_{\text{ext}}^j(r't'), \quad (20)$$

where  $r$  and  $r'$  are the magnitude of the vectors  $\vec{r}$  and  $\vec{r}'$ , respectively.

If we integrate both sides of the previous equation over  $d\hat{r}$  we find

$$4\pi m_{x,y}^i(r,t) = \sum_j \int dr' \int dt' \sum_{LL_1} \chi^{iLL_1;jL_1L}(rt, r't') B_{\text{ext}}^j(r't'). \quad (21)$$

Thus, the functional derivative given by Eq. (18) could be simplified to

$$\bar{\chi}^{ij}(rt, r't') = 4\pi \frac{\delta m_{x,y}^i[B_{\text{ext}}](rt)}{\delta B_{\text{ext}}^j(r't')} \Big|_{B_{\text{ext}}=0, n_0}, \quad (22)$$

where we define  $\bar{\chi}^{ij} = \sum_{LL_1} \chi^{iLL_1;jL_1L}$ . The same procedure is repeated for the magnetic response function  $\chi_0$  of the Kohn-Sham noninteracting system which involves not only  $B_{\text{ext}}$  but  $B_{\text{eff}}$  as well.<sup>14</sup> As mentioned previously,  $B_{\text{eff}}$  is the magnetic part of the effective Kohn-Sham potential ( $V_{\text{eff}}^\downarrow - V_{\text{eff}}^\uparrow$ ). After a Fourier transform with respect to time we obtain a form that maps our calculation onto the same structure employed many years ago by Lowde and Windsor.<sup>24</sup> This remains often used in recent tight-binding simulations of magnetic excitations,<sup>6,7</sup> where it is found that the scheme accurately reproduces results found through use of a more sophisticated description of the Coulomb integrals. Our derivation elucidates how the structure introduced by Lowde and Windsor emerges from TD-DFT.

We now have

$$\bar{\chi}^{ij}(r, r'; \omega) = \bar{\chi}_0^{ij}(r, r'; \omega) + \sum_{kl} \int dr'' \int dr''' \bar{\chi}_0^{ik}(r, r''; \omega) \times U^{kl}(r'', r'''; \omega) \bar{\chi}^{lj}(r''', r'; \omega), \quad (23)$$

where the integrations are only over the magnitude of  $\vec{r}$  and  $\vec{r}'$ , with the site labeled matrix function shown. The effective Coulomb interaction  $U^{ij}(r, r'; \omega)$  may be expressed as a functional derivative given by

$$U^{ij}(r, r'; \omega) = \frac{\delta B_{\text{eff}}^i(r; \omega)}{4\pi \delta m^j(r'; \omega)} \Big|_{B_{\text{ext}}=0, n_0}. \quad (24)$$

Within the ALDA prescription of the transverse response of the spin system, Eq. (24) simplifies to<sup>28</sup>

$$U^{ij}(r, r'; \omega) = \frac{B_{\text{eff}}^i(r; 0)}{4\pi m_z^i(r; 0)} \delta_{r,r'} \delta_{i,j}. \quad (25)$$

The object in Eq. (25), noted in what follows as  $U_{\text{DFT}}$ , is in the literature often referred to as the exchange and correlation kernel  $K_{\text{xc}}$ . This is, it should be noted, exactly the form derived in Eq. (13) extracted from the sum rule Eq. (10).

From Eq. (25), it is obvious that  $U$  could be considered as a local exchange splitting divided by the magnetization.

#### IV. CALCULATION OF THE KOHN-SHAM SUSCEPTIBILITY

As shown in Eq. (2), the Kohn-Sham dynamical susceptibility is a convolution of two Green functions. The function  $\chi_0$  can be separated into a sum of two terms:  $I_1$ , which involves Green functions that are analytical in the same half complex plane, so  $I_1$  itself is analytic, and then one has

$I_2$ , which is nonanalytic.<sup>6</sup> For positive frequencies,

$$I_1^{ij}(\vec{r}, \vec{r}'; \omega) = \frac{i}{2\pi} \int_{-\infty}^{E_F} dz f(z) [G_{ij}^\downarrow(\vec{r}, \vec{r}'; z + \omega) G_{ji}^\uparrow(\vec{r}', \vec{r}; z) - G_{ji}^{\downarrow*}(\vec{r}', \vec{r}; z) G_{ij}^\uparrow(\vec{r}, \vec{r}'; z - \omega)] \quad (26)$$

and

$$I_2^{ij}(\vec{r}, \vec{r}'; \omega) = \frac{i}{2\pi} \int_{-\infty}^{E_F} dz f(z) [-G_{ij}^\downarrow(\vec{r}, \vec{r}'; z + \omega) \times G_{ij}^{\uparrow*}(\vec{r}, \vec{r}'; z) + G_{ij}^\downarrow(\vec{r}, \vec{r}'; z) G_{ij}^{\uparrow*}(\vec{r}, \vec{r}'; z - \omega)]. \quad (27)$$

Such a separation is attractive since  $I_1$  can be calculated through use of a regular energy contour in the complex plane<sup>29</sup> with a modest  $k$  and energy mesh. In Refs. 6 and 7, the energy contour consists of a line perpendicular to the real axis starting at the Fermi energy and going to infinity. This is, unfortunately, not possible with the KKR method since unwanted core states would then be included. Thus, the lower limit of the energy integration is chosen well below the valence band minimum.  $I_2$  can be calculated along a line parallel to the real axis. This requires usually a very substantial numerical effort since a large number of  $k$  points as well as a dense energy mesh are needed. However, it can be shown that the integration is limited to a small energy controlled by  $\omega$ . In our discussion of spin excitations we are interested in frequencies  $\omega$  small compared to bandwidths, so the integrations involved in  $I_2$  can be carried out readily. The computational effort is thus enormously reduced. Upon introducing a variable change, we may write

$$I_2^{ij}(\vec{r}, \vec{r}'; \omega) = -\frac{i}{2\pi} \int_{E_F-\omega}^{E_F} dz G_{ij}^\downarrow(\vec{r}, \vec{r}'; z + \omega) G_{ij}^{\uparrow*}(\vec{r}, \vec{r}'; z). \quad (28)$$

The use of two different contours can lead to a slightly different treatment of rather similar terms in  $I_1$  and  $I_2$ . In order to improve numerical stability, in the present analysis the two terms are arranged so they differ a bit from those presented in Ref. 6. We write

$$I_1^{ij}(\vec{r}, \vec{r}'; \omega) = \frac{i}{2\pi} \int_{-\infty}^{E_F-\omega} dz [f(z) G_{ij}^\downarrow(\vec{r}, \vec{r}'; z + \omega) G_{ji}^\uparrow(\vec{r}', \vec{r}; z) - f(z + \omega) G_{ji}^{\downarrow*}(\vec{r}', \vec{r}; z + \omega) G_{ij}^{\uparrow*}(\vec{r}, \vec{r}'; z)] + \frac{i}{2\pi} \int_{E_F-\omega}^{E_F} dz f(z) G_{ij}^\downarrow(\vec{r}, \vec{r}'; z + \omega) G_{ji}^\uparrow(\vec{r}', \vec{r}; z). \quad (29)$$

The second term on the right-hand side of the previous equation can be added to  $I_2$ , which leads to

$$\bar{I}_2^{ij}(\vec{r}, \vec{r}'; \omega) = \frac{i}{2\pi} \int_{E_F-\omega}^{E_F} dz G_{ij}^\downarrow(\vec{r}, \vec{r}'; z + \omega) [G_{ji}^\uparrow(\vec{r}', \vec{r}; z) - G_{ij}^{\uparrow*}(\vec{r}, \vec{r}'; z)], \quad (30)$$

while

$$\bar{I}_1^{ij}(\vec{r}, \vec{r}'; \omega) = \frac{i}{2\pi} \int_{-\infty}^{E_F-\omega} dz [f(z) G_{ij}^\downarrow(\vec{r}, \vec{r}'; z + \omega) G_{ji}^\uparrow(\vec{r}', \vec{r}; z) - f(z + \omega) G_{ji}^{\downarrow*}(\vec{r}', \vec{r}; z + \omega) G_{ij}^{\uparrow*}(\vec{r}, \vec{r}'; z)] \quad (31)$$



or

$$\bar{I}_1^j(\vec{r}, \vec{r}'; \omega) = \frac{i}{2\pi} \int_{-E_F}^{E_F} dz [f(z - \omega) G_{ij}^\downarrow(\vec{r}, \vec{r}'; z) G_{ji}^\uparrow(\vec{r}', \vec{r}; z - \omega) - f(z) G_{ji}^{\downarrow*}(\vec{r}', \vec{r}; z) G_{ij}^{\uparrow*}(\vec{r}, \vec{r}'; z - \omega)]. \quad (32)$$

This procedure just outlined is found to be stable and requires calculating one less Green function. Up to now we have considered positive frequencies  $\omega$ .

Negative frequencies lead to slightly different forms of  $I_1$  and  $I_2$ :

$$\bar{I}_1^{ij}(\vec{r}, \vec{r}'; -|\omega|) = \frac{i}{2\pi} \int_{-E_F}^{E_F} dz [f(z) G_{ij}^\downarrow(\vec{r}, \vec{r}'; z - |\omega|) G_{ji}^\uparrow(\vec{r}', \vec{r}; z) - f(z - |\omega|) G_{ji}^{\downarrow*}(\vec{r}', \vec{r}; z - |\omega|) G_{ij}^{\uparrow*}(\vec{r}, \vec{r}'; z)] \quad (33)$$

and

$$\begin{aligned} \bar{I}_2^{ij}(\vec{r}, \vec{r}'; -|\omega|) &= \frac{i}{2\pi} \int_{E_F - |\omega|}^{E_F} dz G_{ij}^{\uparrow*}(\vec{r}, \vec{r}'; z + |\omega|) [G_{ij}^\downarrow(\vec{r}, \vec{r}'; z) - G_{ji}^{\downarrow*}(\vec{r}', \vec{r}; z)]. \end{aligned} \quad (34)$$

These expressions can be evaluated with modest numerical efforts since the required Green functions are the same as those calculated for the susceptibilities at positive frequencies.

## V. AN APPROXIMATE FORM FOR THE SINGLE-PARTICLE GREEN FUNCTIONS

The Green functions are provided by the KKR-GF method:<sup>26</sup>

$$\begin{aligned} G_{ij}(\vec{r}, \vec{r}'; z) &= \sum_{LL_1} -i\sqrt{z} R^{iL}(\vec{r}_{<}; z) H^{iL}(\vec{r}_{>}; z) \delta_{ij, LL_1} \\ &\quad + R^{iL}(\vec{r}; z) G_B^{iL, jL_1}(z) R^{jL_1}(\vec{r}'; z), \end{aligned} \quad (35)$$

where  $G_B$  is the structural Green function. Here the regular  $R$  and irregular  $H$  solutions of the Schrödinger equation are energy dependent, and this makes the calculation of  $\chi_0$  in Eq. (1) tedious and lengthy. Thus, instead of using Eq. (35) while evaluating  $\chi_0$ , we introduce the following simplification that captures the physics central to the systems of interest to us.

In its spectral representation, the Green function is given by

$$G_{ij}(\vec{r}, \vec{r}'; z) = \sum_{\vec{k}} \sum_{LL_1} \frac{\alpha_L^i(E_{\vec{k}}) R_L^i(\vec{r}; E_{\vec{k}}) \alpha_{L_1}^{j*}(E_{\vec{k}}) R_{L_1}^{j*}(\vec{r}'; E_{\vec{k}})}{z - E_{\vec{k}}}, \quad (36)$$

where  $R_L^i(\vec{r}; E_{\vec{k}})$  is a suitably normalized solution of the Schrödinger equation within the unit cell  $i$ .  $E_{\vec{k}}$  are the eigenvalues corresponding to the eigenstates of the system, while  $\vec{k}$ , which includes a band index, is a vector in the Brillouin zone of the reciprocal lattice.

Various ansätze can be proposed to simplify the previous form. Instead of working with the energy-dependent wave functions, one could use an energy linearized form of the wave function as done, for example, in the linear muffin tin orbital

method<sup>30</sup> or in the full potential linearized augmented plane waves method.<sup>31</sup> Our ansatz expresses the Green functions in terms of energy-independent wave functions  $\phi$  such that

$$G_{ij}(\vec{r}, \vec{r}'; z) \sim \sum_{\vec{k}} \sum_{LL_1} \frac{\beta_L^i(E_{\vec{k}}) \phi_L^i(\vec{r}) \beta_{L_1}^{j*}(E_{\vec{k}}) \phi_{L_1}^{j*}(\vec{r}')}{z - E_{\vec{k}}} \quad (37)$$

or

$$G_{ij}(\vec{r}, \vec{r}'; z) \sim \sum_{LL_1} \phi_L^i(\vec{r}) \bar{G}_{ij}^{LL_1}(z) \phi_{L_1}^{j*}(\vec{r}'), \quad (38)$$

with

$$\bar{G}_{ij}^{LL_1}(z) = \sum_{\vec{k}} \frac{\beta_L^i(E_{\vec{k}}) \beta_{L_1}^{j*}(E_{\vec{k}})}{z - E_{\vec{k}}}. \quad (39)$$

Note that after modifying the wave functions we naturally replaced the amplitude  $\alpha$  with a different one ( $\beta$ ).

Since our KKR-GF method generates the full Green function as given in Eq. (35), one could calculate  $\bar{G}_{ij}^{LL_1}(z)$  from

$$\bar{G}_{ij}^{LL_1}(z) = \frac{\iint d\vec{r} d\vec{r}' \phi^{iL*}(\vec{r}) G_{ij}(\vec{r}, \vec{r}'; z) \phi^{jL_1}(\vec{r}')}{\int d\vec{r} \phi^{iL*}(\vec{r}) \phi^{iL}(\vec{r}) \int d\vec{r}' \phi^{jL_1}(\vec{r}') \phi^{jL_1*}(\vec{r}')}, \quad (40)$$

where on the right-hand side of Eq. (40) we insert the full KKR Green function displayed in Eq. (35).

The terms in the denominator are normalization factors. Thus, instead of working with  $\phi^{iL}(\vec{r})$ , we introduce

$$\psi^{iL}(r) = \frac{\phi^{iL}(r)}{(\int d\vec{r} \phi^{iL*}(\vec{r}) \phi^{iL}(\vec{r}))^{\frac{1}{2}}}, \quad (41)$$

where we choose  $\phi^{iL}(r) = R^{id}(r; E_F)$ , that is, the wave function of  $d$  character that is the regular solution [see Eq. (35)] of the Schrödinger equation. Our aim is to generate an approximate form for the single-particle Green function which contains full information on the electronic structure and which also is appropriate for use in generating the dynamical susceptibility. We note that the Coulomb interactions responsible for moment formation are intra-atomic in character, inside the  $3d$  shell. Thus, for the purpose of studying the moment and its dynamics, it will suffice to extract just the  $d$ -like portion of a single-particle Green function. In the ETB method, this is precisely what is done, since the Hamiltonian explicitly incorporates only interactions within the  $3d$  shell. We note that the presence of the  $sp$  band complex expresses itself fully in the ansatz we use here, by virtue of hybridization between the  $d$  and  $sp$  levels. Thus, in Eq. (38) we confine the angular momentum components to the  $L = 2$  states. In the full KKR expression for the Green function, the one-electron wave functions which enter are energy dependent. We propose here an expansion in terms of energy-independent wave functions of  $d$  character that we chose to be the regular solutions of KKR-GF theory evaluated at the Fermi energy. Our focus is on low-energy excitations of  $3d$  moments so as we see in what follows this choice is appropriate.

Within the KKR representation of the Green function,  $\bar{G}_{ij}(z)$  is evaluated from

$$\begin{aligned} \bar{G}_{ij}^{LL_1}(z) = & \sum_{L_2 L_3} \left( -i\sqrt{z} \int_0^{r_{ws}} d\vec{r}' H^{iL_2}(\vec{r}'; z) \psi^{iL}(\vec{r}') \right. \\ & \times \int_0^{r'} d\vec{r} \psi^{iL_1*}(\vec{r}) R^{iL_2}(\vec{r}; z) \delta_{ij, L_2 L_3} \\ & - i\sqrt{z} \int_0^{r_{ws}} d\vec{r}' R^{iL_2}(\vec{r}'; z) \psi^{iL}(\vec{r}') \\ & \times \int_{r'}^{r_{ws}} d\vec{r} \psi^{iL_1*}(\vec{r}) H^{iL_2}(\vec{r}; z) \delta_{ij, L_2 L_3} \\ & + \int_0^{r_{ws}} d\vec{r} \psi^{iL*}(\vec{r}) R^{iL_2}(\vec{r}; z) G_B^{iL_2, jL_3}(z) \\ & \left. \times \int_0^{r_{ws}} d\vec{r}' R^{jL_3}(\vec{r}'; z) \psi^{jL_1}(\vec{r}') \right), \end{aligned} \quad (42)$$

where  $r_{ws}$  stands for Wigner-Seitz radius.

## VI. THE FINAL DYSON EQUATION

Assuming the expansion in terms of energy-independent wave functions described previously, the final Dyson equation simplifies after some straightforward algebra into a strictly site-dependent equation,

$$\bar{\chi} = \bar{\chi}_0 + \bar{\chi}_0 \bar{U} \bar{\chi}, \quad (43)$$

where the  $d$  block of the dynamical susceptibility is given by

$$\bar{\chi}_0^{ij}(r, r'; \omega) = \psi_{\downarrow}^{id}(r) \psi_{\uparrow}^{id*}(r) \bar{\chi}_0^{ij}(\omega) \psi_{\downarrow}^{jd*}(r') \psi_{\uparrow}^{jd}(r') \quad (44)$$

and

$$\bar{U}^i = \int_0^{r_{ws}} dr \psi_{\downarrow}^{id*}(r) \psi_{\uparrow}^{id}(r) U^i(r) \psi_{\downarrow}^{id}(r) \psi_{\uparrow}^{id*}(r). \quad (45)$$

Within ALDA, we use Eq. (25) in Eq. (45) and obtain

$$\bar{U}^i = \int_0^{r_{ws}} dr \psi_{\downarrow}^{id*}(r) \psi_{\uparrow}^{id}(r) \frac{B_{\text{eff}}^i(r; 0)}{4\pi m_z^i(r; 0)} \psi_{\downarrow}^{id}(r) \psi_{\uparrow}^{id*}(r). \quad (46)$$

If we want to use the sum rule we expand the susceptibility given in Eq. (12) in terms of  $d$ -block susceptibility expressed in Eq. (44) and repeat the same procedure used in Sec. II to find

$$\bar{U} = \bar{\Gamma}^{-1} \bar{M}_z, \quad (47)$$

as written in matrix notation and  $\bar{\Gamma}^{ij} = \bar{\chi}_0^{ij}(0) M_z^j$  with  $M_z^i$ , calculated from the projection scheme proposed in Sec. V, is the magnetic moment of atom  $i$ .  $\bar{U}$  can be calculated once for every atom either from the previous sum rule, Eq. (47), or from Eq. (46). It can be understood as a Stoner parameter and gives once more a justification for the approach used by Lowde and Windsor;<sup>24</sup> that is, the effective intra-atomic Coulomb interaction is expressed by only one parameter.

## VII. APPLICATION OF THE FORMALISM TO EXPLICIT EXAMPLES

### A. Single adatoms

We choose as an application of the formalism developed earlier the investigation of 3d adatoms and dimers positioned on the fourfold hollow sites of Cu(001) surface. In this section, we focus on single adatoms. The calculations consist of the self-consistent determination of the electronic structure of these nanostructures using the usual KKR-GF scheme.<sup>26</sup> Once this is done, we generate the Green functions needed to calculate  $\chi_0$ , for the elements that bear magnetic moments (Cr, Mn, Fe, and Co), following Eq. (2).  $U$  is calculated either from Eq. (47) or Eq. (46). It is convenient to note that for the case of a single adatom  $i$ , Eq. (47) simplifies to  $U_i = \frac{1}{\chi_0^i}$  at  $\omega = 0$ .

We have already examined the spin dynamics of these systems in Ref. 21, where we have shown that the Green functions extracted from our approach [Eq. (43)] nicely reproduce the magnetic moment of the adatoms as calculated from a full DFT calculation. That this is so is illustrated in Fig. 1(a). Indeed, interestingly, the  $d$  contribution to the total moment is, as expected, the most important and seems to be nicely reproduced by the projection of the Green functions into our choice of wave functions.

We did not, however, discuss in Ref. 21 the differences between values of  $U$  calculated from both schemes mentioned previously. In Fig. 1(b) we show the values of  $U$  for the

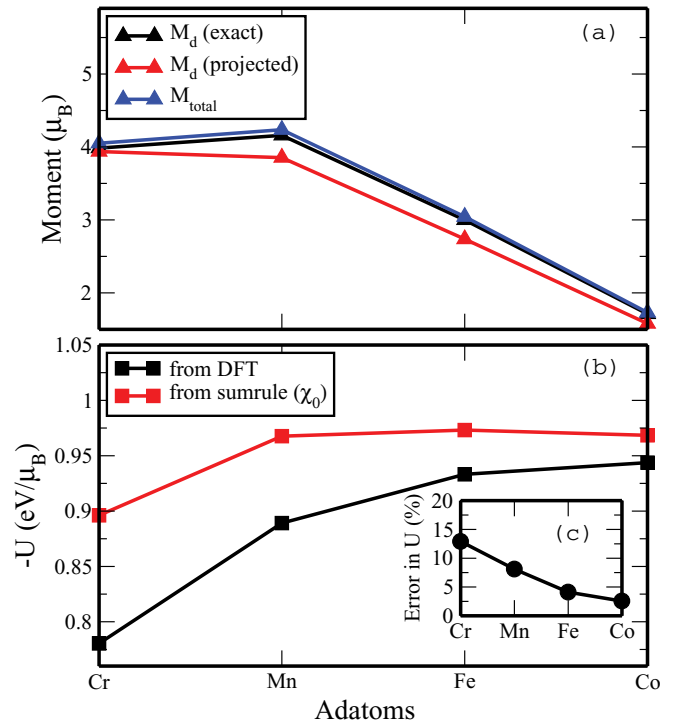


FIG. 1. (Color online) (a) Comparison between magnetic moments (in  $\mu_B$ ) of adatoms calculated by the full KKR-GF with those calculated from the proposed projection scheme discussed in the text and in Ref. 21. Values of  $-U$  ( $\text{eV}/\mu_B$ ) are shown in panel (b) calculated from either from Eq. (47) or from Eq. (46), while in the inset (c) we plot the percentage error defined as the difference between  $U_{\text{DFT}}$  and  $U_{\text{sumrule}}$  divided by  $U_{\text{DFT}}$ .

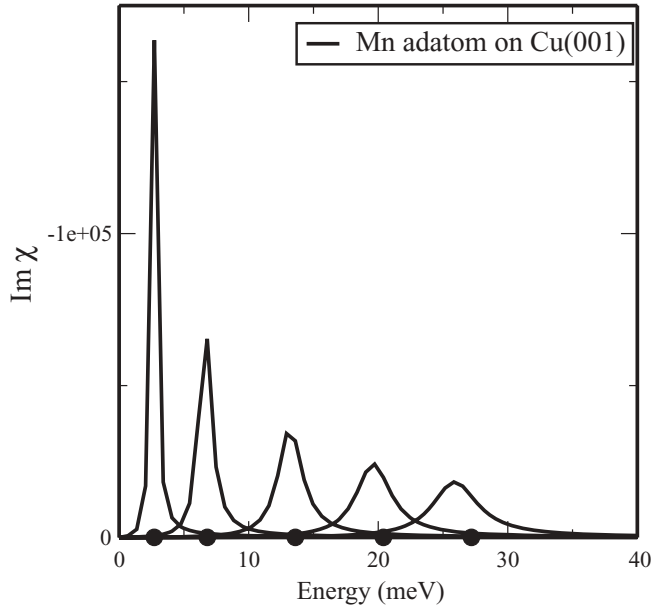


FIG. 2. Imaginary part of the transverse dynamical magnetic susceptibility for a Mn adatom/Cu(001) surface. After applying different dc magnetic fields, resonances are obtained and shifted to higher frequencies by increasing the magnitude of the field. The corresponding Zeeman frequencies with  $g = 2$  for the fields chosen are represented by the black circles. Thus, the  $g$  shift is negative for this example.

adatoms we have investigated. We find values of  $U$  very close to  $1 \text{ eV}/\mu_B$  for all cases we have studied. Himpsel,<sup>25</sup> in his analysis of a large body of photoemission data on moment-bearing  $3d$  ions, has concluded that  $1 \text{ eV}/\mu_B$  is a universal value that applies to diverse moment-bearing  $3d$  transition-metal ions. As discussed in Ref. 21,  $1 \text{ eV}/\mu_B$  is also used commonly in ETB calculations.<sup>6,7</sup> Thus, we are pleased to see these values emerge from the scheme set forth here. The relative error or  $U$  values generated from DFT, as measured by the ratio  $(\frac{U_{\text{DFT}} - U_{\text{sumrule}}}{U_{\text{DFT}}})$  are depicted in Fig. 1(c). The error is the highest for Cr adatom, while the lowest is seen for Co. It is interesting that the observed error does not exceed 15%, which is still much lower than what has been estimated by Sasioglu *et al.*<sup>23</sup> while investigating bulk Ni.

In Fig. 2, we show examples of the imaginary part of  $\chi$  for a Mn adatom positioned on the fourfold hollow site of Cu(001) surface after applying an additional spatially uniform static magnetic field. The imaginary part of  $\chi$  describes the resonant response of the local magnetic moment of Mn adatom. As required by the Goldstone theorem, a zero-frequency resonance is expected when no dc field is applied. We have verified numerically that this feature is present when our method of determining  $U$  is employed. As soon as a dc field pointing along the initial direction of the moment is applied, as discussed many years ago,<sup>32</sup> the local response of the moment displays a  $g$ -shifted Zeeman resonance, broadened very substantially by decay of the coherent spin precession to particle-hole pairs, whereas the total moment of the system precesses with  $g = 2$  and zero linewidth. Thus, experiments such as STM that are highly localized probes of the dynamic response of the moment see a qualitatively different response

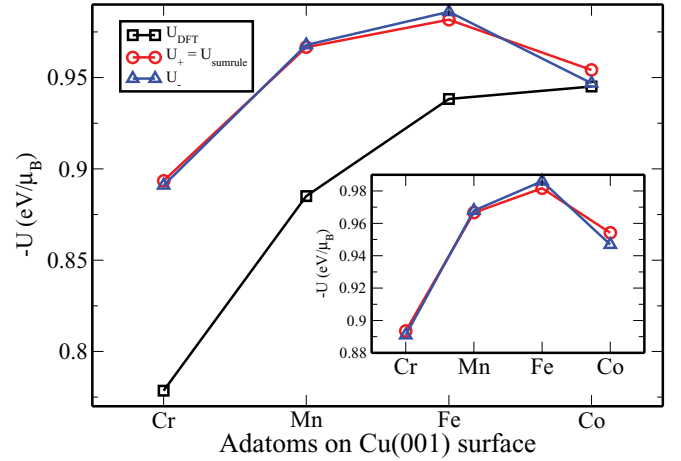


FIG. 3. (Color online) Different values of  $U$  obtained with different schemes for Cr, Mn, Fe, and Co dimers deposited on a Cu(001) surface. See the text for a discussion of the various criteria for choosing  $U$ .

than very-long-wavelength probes such as microwave resonance or Brillouin light scattering. In the latter methods, both  $g$  shifts and linewidths have their origin only in terms in the system Hamiltonian that break spin rotation invariance. Examples are spin-orbit effects, along with coupling of spins to lattice degrees of freedom.

We see in Fig. 2 that the resonant frequency scales linearly with the applied dc field, as does the width of the structure in the local response of the moment. The width of the resonances is controlled by the local density of states,<sup>32</sup> and is thus strongly influenced by the position of the  $d$  levels relative to the Fermi energy.

## B. Dimers of identical adatoms

Let us turn to the case of dimers. We consider two identical adatoms, each adsorbed in nearest-neighbor fourfold hollow sites on Cu(100). At such distances, their interaction is modest compared to energies which characterize the one-electron properties of the system.

In Fig. 3, we show effective values of  $U$  generated by different means of selecting this parameter. The one calculated with use of Eq. (46), referred to as  $U_{\text{DFT}}$ , is systematically smaller than that which follows from the sum rule in Eq. (47). We saw the same trend in our earlier discussion of single adatoms. Of course, if one employs  $U_{\text{DFT}}$  in the calculation of the dynamic susceptibility, the Goldstone theorem is not obeyed. We turn next to a discussion of the two choices  $U_+$  and  $U_-$  that appear in Fig. 3.

We discuss local dynamic susceptibilities  $\chi^{11}$ ,  $\chi^{22}$ ,  $\chi^{12}$ , and  $\chi^{21}$ . The superscripts refer to atomic sites where the atoms in the dimer are located. The response function  $\chi^{ij}$  gives the response of the moment at site  $i$  in response to a spatially localized field applied to site  $j$ . So far, everywhere, upper-case letters were used for  $i$  and  $j$  site labels in the susceptibility. For the case considered in this section, where each atom in the dimer is identical and there is reflection symmetry through the midpoint of the line that connects their centers, we have  $\chi^{11} = \chi^{22}$  and also  $\chi^{21} = \chi^{12}$ . In the next section we consider

a dimer formed from two dissimilar atoms, so the equalities just stated do not hold.

The Goldstone theorem requires that in the absence of an externally applied field (and in the absence of spin-orbit coupling), each element  $\chi^{ij}$  must have a pole at zero frequency. This is ensured if  $U$  is such that the determinant  $D$  formed from the matrix  $1 - U\chi_0$  vanishes at zero frequency. For our dimer that consists of two identical atoms we have  $D = (1 - U\chi_0^{11})^2 + (U\chi_0^{12})^2$ . Upon setting  $D = 0$ , we encounter a difficulty. The criterion yields two acceptable values of  $U$ ,  $U_+ = (\chi_0^{11} + \chi_0^{12})^{-1}$  and  $U_- = (\chi_0^{11} - \chi_0^{12})^{-1}$ . In Fig. 3, the red curve with circles provides values of  $U_+$ , for the ions we consider and the blue curve with triangles  $U_-$ . The two values of  $U$  determined by this criterion are quite close to each other because on the electron-volt scale the interaction energy between the two moments in the dimer is quite small, as noted earlier.

One then must address which of the two choices for  $U$  discussed in the previous paragraph is the proper physical choice. To see this, we must refine our criterion. For the dimer with two identical atoms, we can make a decision about which value of  $U$  is the proper choice. If we consider the mode structure of the dimer, there is an acoustical mode wherein the two moments precess in phase, and we discuss an out-of-phase optical mode in what follows. The Goldstone theorem requires the acoustical mode to have zero frequency. Thus, it is the function  $\chi^a = \chi^{11} + \chi^{22} + \chi^{12} + \chi^{21}$  that also must have a pole at zero frequency, since this describes the response of the total moment of the dimer to a spatially uniform applied transverse field. For our simple dimer formed from two identical atoms, it is a simple exercise to find an expression for  $\chi^a$ . One has  $\chi^a = (\chi_0^{11} + \chi_0^{12})/[1 - U(\chi_0^{11} + \chi_0^{12})]$ . Thus, for a pole to occur at zero frequency in this response function, we must choose  $U = U_+$ . The sum rule provides us with the same criterion.

For the case of the dimer just considered, it is straightforward to deduce the appropriate choice of  $U$  through examination of  $\chi^a$ . However, for more complex arrays of spins the task of choosing  $U$  is not simple. Suppose, for instance, we have  $N$  spins in the form of a one-dimensional structure or possibly an island. From the numerical point of view, one may work with the analog of the determinant  $D$  discussed earlier. Exploration of its zeros at zero frequency will yield  $N$  possible values of  $U$ . Also if the spin structure consists of dissimilar atoms, each atom will be characterized by an appropriate value of  $U$ . As we see in the next section, the sum rule allows one to generate appropriate values of the interaction strength for each individual atom in a more complex structure.

We turn next to the description of the spin dynamics of the dimer. For the dimer, we expect two resonances, an acoustical mode located obviously at  $\omega = 0$  and an optical mode at positive or negative frequencies. In general, the appearance of negative frequency modes in the dynamic susceptibility signal an instability of an assumed ground state. In the studies presented here, we assume a ferromagnetic ground state for the dimer. The appearance of a negative-frequency optical mode is a signal that the atoms in the dimer are coupled antiferromagnetically, so the ferromagnetic ground state is unstable. Thus, the dynamic susceptibility can be used as a probe of local stability of assumed structures.

It will be useful and interesting to compare our full dynamical calculations of the response of the dimer with the often used localized spin model, where effective exchange interactions are calculated within an adiabatic scheme. Such an adiabatic scheme has already been used for the investigation of different kinds of systems (see, e.g., Refs. 33–36). Through adiabatic rotations of the moments,<sup>27</sup> we extract an effective exchange magnetic interaction,  $J$ , by fitting the energy change to the Heisenberg form,

$$H = -J\vec{e}_1 \cdot \vec{e}_2, \quad (48)$$

where  $\vec{e}_1$  and  $\vec{e}_2$  are unit vectors. Using this criterion, we find that the ground state is antiferromagnetic for Cr ( $J = -19.8$  meV) and Co dimers ( $J = -14.9$  meV) and ferromagnetic for Mn ( $J = 16.3$  meV) and Fe ( $J = 30.4$  meV). Since the dynamical susceptibility was evaluated through use of ferromagnetic state for all the dimers, we expect an optical mode at positive frequencies for Mn and Fe dimers and at negative frequencies for Cr and Co dimers.

We find that the dynamic susceptibility of the dimer is remarkably sensitive to the choice of the effective  $U$ . We see in Fig. 3 that numerically the difference between  $U_+ (= U_{\text{sumrule}})$  and  $U_-$  is quite small. Yet, as illustrated in Fig. 4(a), we show  $\text{Im}(\chi^{11})$  calculated with the choice  $U = U_-$ . For all four magnetic ions, the signature of the Goldstone mode is evident. For the Cr dimer, we see the clear signature of the optical mode at positive frequency. This suggests that, in contrast to the conclusion based on the adiabatic exchange analysis, the

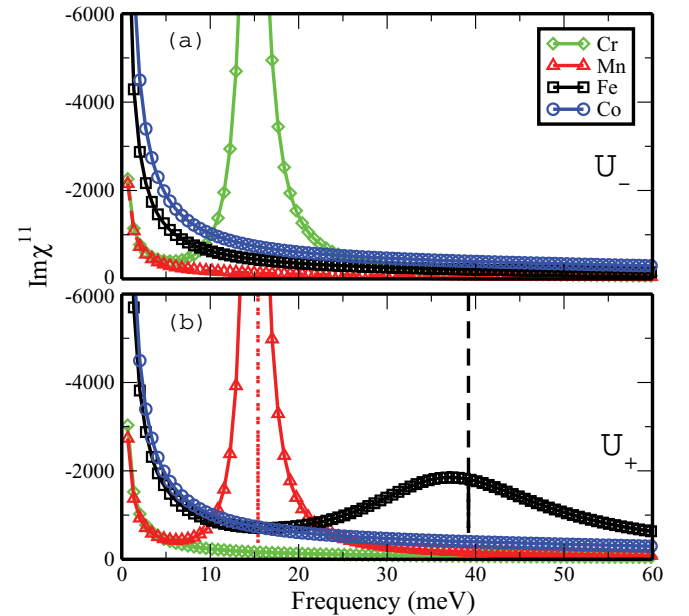


FIG. 4. (Color online) Local  $\text{Im}\chi^{11}$  is shown for the four dimers based on Cr, Mn, Fe, and Co adatoms. To calculate  $\chi$  two possible schemes of evaluating are considered: in (a) using  $U_-$  and in (b) using  $U_+$ . It turns out that  $U_+$  corresponds to the value obtained from the sum rule [Eq. (47)] derived in the text while  $U_-$  that calculated from a simple iterative scheme out of  $U_{\text{DFT}}$  would converge to the wrong  $U$  when investigating Cr and Co dimers. The reason is that, for the latter elements, contrary to  $U_+$ ,  $U_-$  is closer to  $U_{\text{DFT}}$ . The optical modes, estimated for Mn and Fe from a Heisenberg model, are represented as dashed lines.



ferromagnetic ground state of Cr is stable. The optical modes of Mn and Fe all reside at negative frequency, so for these three the results in Fig. 4(a) suggest the ferromagnetic ground state is unstable. These results are also incompatible with the conclusions based on the adiabatic exchange integrals.

In Fig. 4(b), we show results for  $\text{Im}(\chi^{11})$  which follow from the choice  $U = U_+$ . We now have results fully compatible with the conclusion based on the adiabatic exchange analysis. The sum rule has led to the correct selection of the effective  $U$ .

Within the framework of the Heisenberg model, the optical mode should be an eigenmode of the system, and thus it will have zero linewidth. We see in Fig. 4(b) that the optical mode for the Fe dimer and the Mn dimer have very substantial width. The origin of this broadening is in the decay of the optical mode to Stoner excitations. The itinerant character of the local moments is responsible for this linewidth, which elementary considerations suggest should increase linearly with the frequency of the optical mode. Thus, the linewidth of the optical mode of the Fe dimer is substantially broader than that of the Mn dimer. In the ground state, hybridization between  $3d$  states of the adatom and the conduction degrees of freedom on the Cu substrate results in “virtual levels” whose width is in the range of a few hundred meV. At the level of the spin dynamics, we see the large broadening of the optical mode as another reflection of the itinerant character of these systems. We note that in spin-polarized electron energy loss spectroscopy studies of spin waves in ultrathin films very large linewidths are observed for high-frequency, large-wave-vector modes.<sup>37</sup> The data are in excellent accord with theoretical calculations that assign the large linewidth to the damping by decay to Stoner excitations,<sup>7</sup> very much as we see in the optical modes displayed in Fig. 4(b).

It is of interest to compare the frequency of the optical modes with the prediction of the Heisenberg model, with interspin exchange generated adiabatically as discussed earlier. If one considers two spin-exchange-coupled spins described by the Hamiltonian  $-J_s \vec{S}_1 \cdot \vec{S}_2$ , the frequency of the optical mode is easily seen to be  $J_s(S_1 + S_2)$ . In Eq. (48),  $\vec{e}_{1,2}$  are unit vectors, so  $J_s = J/S_1 S_2$ . Thus, in terms of the effective exchange couplings quoted earlier, with  $S_1 = S_2 = S$  the optical mode frequency is  $2J/S$ . For the Mn and Fe dimers whose optical modes are illustrated in Fig. 4(b), the predicted frequencies are 15.4 and 39.2 meV, respectively. The agreement with the optical mode of the Mn dimer is excellent, whereas the full dynamical calculation provides a somewhat smaller optical mode frequency for the Fe dimer. As discussed earlier, the coupling between the spin precession of the local moments and the Stoner excitations produces a mode softening not incorporated into the localized spin picture.<sup>6,7</sup> This coupling is considerably larger for the Fe dimer than the Mn dimer, as seen by a comparison of their linewidths.

### C. Dimers formed from different adatoms

We now turn our attention to a lower-symmetry spin structure, dimers made of different magnetic adatoms. We study the MnFe dimer and the FeCo dimer, once again with the magnetic ions sitting in nearest-neighbor fourfold hollow sites on the Cu(111) surface. Here the two atoms do not have the same magnetic moments. Also, the effective  $U$  is

TABLE I. Comparison between magnetic moments (in  $\mu_B$ ) and values of  $U$ 's (eV/ $\mu_B$ ) for dimers made of different adatoms: MnFe and FeCo dimers.

	Mn/Fe	Fe/Co
$M_d$ , projection model	3.85/2.74	2.78/1.64
$M_{\text{total}}$	4.23/3.06	3.13/1.82
$-U_{\text{DFT}}$	0.89/0.94	0.94/0.95
$-U_{\text{sumrule}}$	0.97/0.98	0.98/0.98

different for each atom. In this circumstance it is difficult to envision adjusting the values of  $U$  by hand to obtain the zero-frequency pole in the dynamic susceptibility. We have here a circumstance where the sum rule allows us to address the problem directly. Notice from Eq. (47) that, through its use, we can determine the appropriate value of  $U$  for each atom in the dimer. Before we discuss the imaginary part of the dynamical susceptibility, let us discuss values of the magnetic moments and  $U$ 's.

In Table I, the magnetic moments calculated with our projection scheme are shown and compared to the values that follow from the full KKR treatment of the ground state. In the first line of Table I the moment which appears is the contribution with  $d$ -like symmetry, since this is the portion built into our ansatz for the Green function used to compute the Khon-Sham susceptibility. It is interesting to note the substantial difference between the magnetic moments of two adatoms in the dimer. It is the case here as for the single adatom, the  $U$  calculated from Eq. (46) underestimates the value of  $U$  needed to realize the Goldstone mode. From Eq. (47), we may deduce the value  $U$ , for each of the adatoms in the dimer. We find

$$U_1 = \frac{\frac{m_z^2}{m_z^2} \chi_0^{12} - \chi_0^{22}}{\chi_0^{12} \chi_0^{21} - \chi_0^{11} \chi_0^{22}} \quad (49)$$

and

$$U_2 = \frac{\frac{m_z^2}{m_z^2} \chi_0^{21} - \chi_0^{11}}{\chi_0^{12} \chi_0^{21} - \chi_0^{11} \chi_0^{22}}. \quad (50)$$

It is interesting that the sum rule gives similar values of  $U$  for both atoms in the dimer and also that  $U$  is very close to 1 eV/ $\mu_B$ . That this is so is very compatible with the conclusion of Ref. 25, which is based on an empirical study of photoemission data on  $3d$  transition-metal ions in diverse environments.

The mapping to the previously defined Heisenberg model predicts a ferromagnetic ground state for both dimers investigated. Indeed, the magnetic exchange interaction is positive in both cases with  $J_{\text{MnFe}} = 28.1$  meV (Heisenberg frequency, 31.6 meV) and  $J_{\text{FeCo}} = 12.5$  meV (Heisenberg frequency, 21.7 meV). This indicates, as discussed earlier, that the imaginary part of the dynamical magnetic susceptibility for every adatom should show a resonance at positive frequencies that is the signature of the optical mode. In Figs. 5(a) and 5(b) we plot  $\chi^{11}$  and  $\chi^{22}$ , respectively, for the FeCo and MnFe dimer.

A most striking feature of the results displayed in Fig. 5 is that the peak positions in  $\chi^{11}$  and  $\chi^{22}$  occur at distinctly

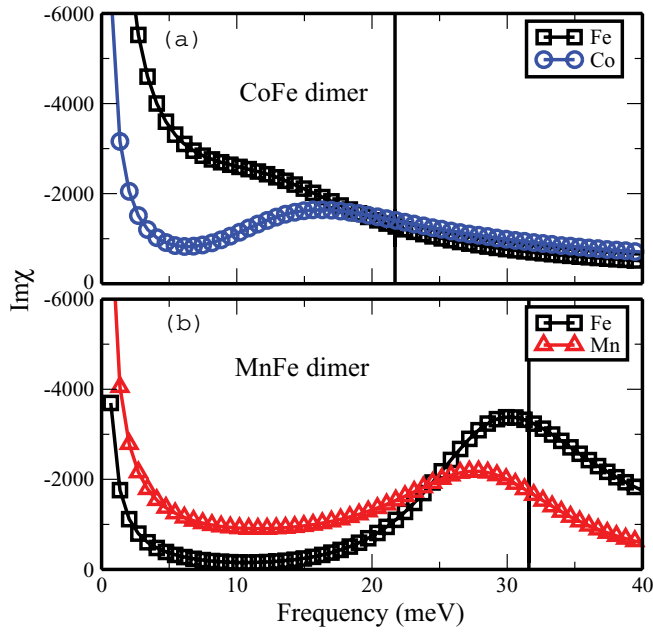


FIG. 5. (Color online) Local  $\text{Im}\chi$  for dimers with mixed adatoms are shown in (a) for FeCo dimer and in (b) for MnFe dimer. Equation (47) based on the sum rule derived in the text was used to define  $U$ . It is interesting to note the presence of resonances at positive frequencies expressing a ferromagnetic ground state for both dimers. Within each dimer, the peaks related to every adatom are not located at the same position since the  $g$  shift depends on the nature of the adatom.

different frequencies. This is particularly clear in Fig. 5(b), where the influence of damping is somewhat more modest than in Fig. 5(a). We see that the peak in  $\chi^{\text{FeFe}}$  occurs at 30 meV, whereas that in  $\chi^{\text{MnMn}}$  is distinctly downshifted to 27 meV.

This behavior is at variance with the Heisenberg description of the excitation spectrum of two well-defined localized spins. As we have seen, if we have two well-defined, localized spins coupled together by the exchange interaction  $-J\vec{e}_1 \cdot \vec{e}_2$ , the pair has two excited states associated with small-amplitude motions, the acoustical mode at zero frequency (which we see in Fig. 5), and the optical mode at the frequency  $2J/S$ . Thus, the optical mode peak in the excitation spectrum for each member of the dimer should be at exactly the same frequency, in this picture. While the oscillator strength of each peak will differ, there is a unique excited-state energy of the pair.

The shift in the peak positions evident in Fig. 5 is a consequence of the itinerant nature of the magnetic moments. As each moment precesses, as we have seen, the motion is damped heavily by the coupling of the moment to the Stoner excitations of the paramagnetic host. In the case of the FeMn dimer, the motions of the Fe spin are damped far more heavily than those of the Mn spin, as we may appreciate from Fig. 1(b) of Ref. 21. This has the consequence that the peak in  $\text{Im}\chi^{\text{MnMn}}$  is dragged down to a frequency somewhat lower than that in  $\text{Im}\chi^{\text{FeFe}}$ . We may see this by constructing a toy model that consists of two Heisenberg coupled spins, each of which is coupled to a reservoir that produces damping  $\alpha$  of the form encountered in the Landau-Lifschitz-Gilbert equation. The linearized equations of motion for this system reproduce the offset in the peaks evident in Fig. 5(b). We illustrate this in Fig. 6 where  $\text{Im}\chi^{11}$  and  $\text{Im}\chi^{22}$  mimic the imaginary parts of

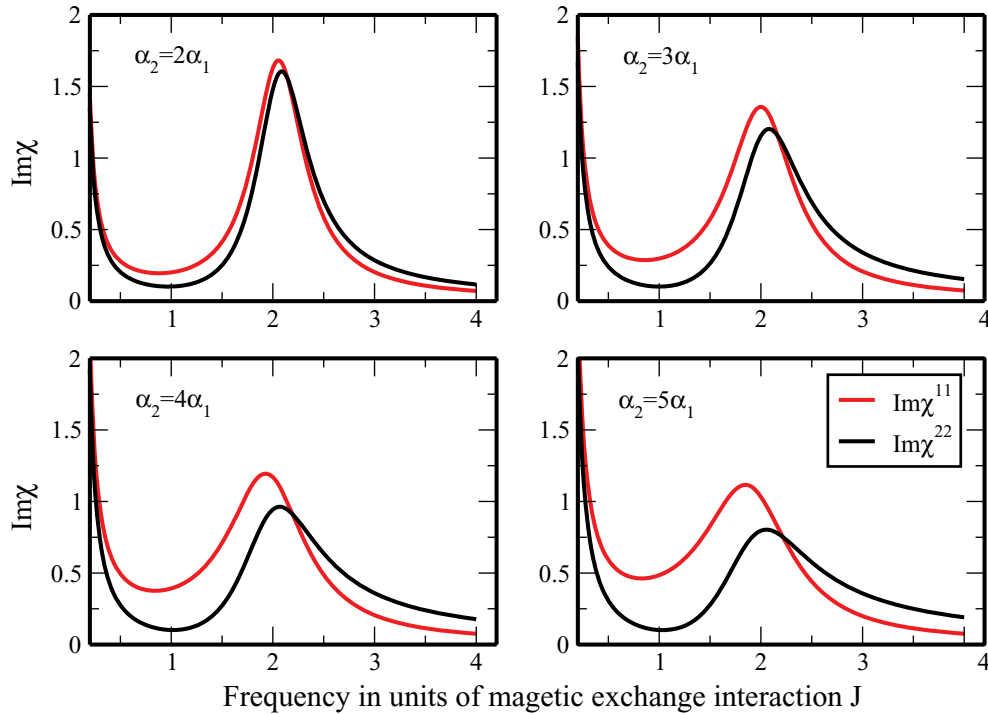


FIG. 6. (Color online) The response function  $\text{Im}(\chi^{11})$  and  $\text{Im}(\chi^{22})$  for two spins of unit length coupled by an exchange interaction of strength  $J = 1$ . Here we mimic Fe and Mn by considering each spin coupled to a reservoir that provides a damping parameter  $\alpha_{1,2}$  (1 for Mn and 2 for Fe) whose values are given in the inset.

$\chi^{\text{MnMn}}$  and  $\chi^{\text{FeFe}}$ . By increasing the strength of the damping parameter  $\alpha_2$  compared to  $\alpha_1$ , we observe a shift to lower energies of the optical mode in  $\text{Im}\chi^{22}$  (i.e.,  $\text{Im}\chi^{\text{MnMn}}$ ). It is striking to observe the completely different shape of the optical mode of Mn spin just by modifying a neighbor. Indeed, by comparing the optical mode observed in  $\text{Im}\chi^{\text{MnMn}}$  we observe also that it is much more heavily damped in the mixed dimer MnFe [Fig. 5(b)] than in the pure MnMn dimer [Fig. 4(b)]. The physical reason behind this intriguing behavior is that in the MnFe configuration, the Mn spin during its precession feels the magnetic force of the heavily damped Fe spin which provides more damping on Mn. It would be of great interest to employ STM-based spectroscopy to explore the response of the two spins in a dissimilar dimer such as that just discussed.

### VIII. CONCLUSION

We have developed and presented a theory based on TD-DFT and the KKR-GF method to extract dynamics magnetic susceptibilities of moment bearing adatoms and adatom dimers on surfaces. In our method, the electronic structure is described within an *ab initio* scheme with KKR Green functions as the basis. Thus, no parameters need to be introduced, as in studies that employ the ETB method. An important feature of our approach is that it may be implemented with a modest expenditure of computational effort. It is thus suitable for exploration of complex magnetic structures on surfaces that contain several magnetic ions. In this paper, we illustrate the method with application to magnetic dimers formed from either identical or dissimilar adatoms.

As discussed earlier, a difficulty with past TD-DFT studies of spin excitations not only on surfaces, but in bulk materials as well, is that the effective value of the Hubbard  $U$  which emerges from the standard approaches is not compatible with the Goldstone theorem that guarantees that the low-lying acoustical spin-excitation has zero frequency. This difficulty has led others to make *ad hoc* adjustments in the value of  $U$ . A feature of the present analysis is the introduction of a sum rule from which proper values of this parameter emerge. This eliminates the need for *ad hoc* adjustments. It should be remarked that in simple systems, where the analysis can be phrased in terms of a single value of the effective  $U$ , it is not difficult to ensure satisfaction of the Goldstone theorem through an *ad hoc* correction, though in our view this is an un-

satisfactory procedure that compromises the theory at the fundamental level. Additionally, for a multicomponent system, the *ad hoc* correction procedure becomes problematic in practice. As we see from our discussion of the dimer constructed from two different magnetic ions, our sum-rule approach is readily and easily implemented for multi component systems.

### ACKNOWLEDGMENTS

Research supported by the US Department of Energy through Grant No. DE-FG03-84ER-45083. R.B.M. acknowledges support from CNPq and FAPERJ, Brazil. S.L. thanks the Alexander von Humboldt Foundation for a Feodor Lynen Fellowship and also thanks Stefan Blügel for constant support of this work. The computations were performed at the supercomputer JUROPA at the Forschungszentrum Jülich.

### APPENDIX

In this Appendix we provide a derivation of the useful identity presented in Eq. (6).

The Green function  $G(z)$  of a Hamiltonian operator  $H$  is defined by the operator equation

$$G = \frac{1}{z - H}. \quad (\text{A1})$$

If no spin-orbit coupling and noncollinear magnetism are considered, the previous equation holds for every spin channel ( $\uparrow$  or  $\downarrow$ ). Thus,

$$G^{\uparrow(\downarrow)} = \frac{1}{z - H^{\uparrow(\downarrow)}}. \quad (\text{A2})$$

In addition we have

$$z - H^{\downarrow} = z - H^{\uparrow} + H^{\downarrow} - H^{\uparrow}, \quad (\text{A3})$$

which can be multiplied from both sides, from the left by  $(z - H^{\downarrow})^{-1}$ , and from the right by  $(z - H^{\uparrow})^{-1}$ . This leads to

$$\frac{1}{z - H^{\uparrow}} = \frac{1}{z - H^{\downarrow}} + \frac{1}{z - H^{\downarrow}}(H^{\downarrow} - H^{\uparrow})\frac{1}{z - H^{\uparrow}}; \quad (\text{A4})$$

that is,

$$G^{\uparrow} = G^{\downarrow} + G^{\downarrow} B_{\text{eff}} G^{\uparrow}, \quad (\text{A5})$$

where we define  $B_{\text{eff}} = H^{\downarrow} - H^{\uparrow}$ .

\*On leave from Institut für Festkörperforschung & Institute for Advanced Simulation, Forschungszentrum Jülich & JARA, D-52425 Jülich, Germany; slounis@uci.edu.

<sup>1</sup>A. J. Heinrich, J. A. Gupta, C. P. Lutz, and D. M. Eigler, *Science* **306**, 466 (2004); C. F. Hirjibehedin, C.-Y. Lin, A. F. Otte, M. Ternes, C. P. Lutz, B. A. Jones, and A. J. Heinrich, *ibid.* **317**, 1199 (2007); A. F. Otte, M. Ternes, K. von Bergmann, S. Loth, H. Brune, C. P. Lutz, C. F. Hirjibehedin, and A. J. Heinrich, *Nat. Phys.* **4**, 847 (2008); C. F. Hirjibehedin, C. P. Lutz, and A. J. Heinrich, *Science* **312**, 1021 (2006); S. Loth, K. von Bergmann, M. Ternes, A. F. Otte, C. P. Lutz, and A. J. Heinrich, *Nat. Phys.* **6**, 340 (2010).

<sup>2</sup>T. Balashov, T. Schuh, A. F. Takacs, A. Ernst, S. Ostanin, J. Henk, I. Mertig, P. Bruno, T. Miyamachi, S. Suga, and W. Wulfhekkel, *Phys. Rev. Lett.* **102**, 257203 (2009); T. Schuh, T. Balashov, T. Miyamachi, A. F. Takacs, S. Suga, and W. Wulfhekkel, *J. Appl. Phys.* **107**, 09E156 (2010); T. Balashov, A. F. Takacs, M. Dane, A. Ernst, P. Bruno, and W. Wulfhekkel, *Phys. Rev. B* **78**, 174404 (2008); T. Balashov, A. F. Takacs, W. Wulfhekkel, and J. Kirschner, *Phys. Rev. Lett.* **97**, 187201 (2006).

<sup>3</sup>A. A. Khajetoorians, S. Lounis, B. Chilian, A. T. Costa, L. Zhou, D. L. Mills, R. Wiesendanger, and J. Wiebe (accepted in *Phys. Rev. Lett.*), e-print [arXiv:1010.1284](https://arxiv.org/abs/1010.1284).

- <sup>4</sup>J. F. Cooke, J. A. Blackman, and T. Morgan, *Phys. Rev. Lett.* **54**, 718 (1985).
- <sup>5</sup>H. Tang, M. Plihal, and D. L. Mills, *J. Magn. Magn. Mater.* **187**, 23 (1998).
- <sup>6</sup>R. B. Muniz and D. L. Mills, *Phys. Rev. B* **68**, 224414 (2003); **66**, 174417 (2002).
- <sup>7</sup>A. T. Costa, R. B. Muniz, and D. L. Mills, *Phys. Rev. B* **70**, 054406 (2004); **73**, 054426 (2006); A. T. Costa, R. B. Muniz, S. Lounis, A. B. Klautau, and D. L. Mills, *ibid.* **82**, 014428 (2010); A. T. Costa, R. B. Muniz, and D. L. Mills, *Phys. Rev. Lett.* **94**, 137203 (2005).
- <sup>8</sup>J. Fransson, *Nano Lett.* **9**, 2414 (2009); J. Fransson, H. C. Manoharan, and A. V. Balatsky, *ibid.* **10**, 1600 (2010); J. Fransson, O. Eriksson, and A. V. Balatsky, *Phys. Rev. B* **81**, 115454 (2010).
- <sup>9</sup>A. V. Balatsky, A. Abanov, and J. X. Zhu, *Phys. Rev. B* **68**, 214506 (2003).
- <sup>10</sup>J. Fernandez-Rossier, *Phys. Rev. Lett.* **102**, 256802 (2009); F. Delgado, J. J. Palacios, and J. Fernandez-Rossier, *ibid.* **104**, 026601 (2010).
- <sup>11</sup>N. Lorente and J. P. Gauyacq, *Phys. Rev. Lett.* **103**, 176601 (2009).
- <sup>12</sup>M. Persson, *Phys. Rev. Lett.* **103**, 050801 (2009).
- <sup>13</sup>This is the subject of a future publication including the full theory for simulations of inelastic STM experiments. Reference [8] is useful for this matter as well.
- <sup>14</sup>E. Runge and E. K. U. Gross, *Phys. Rev. Lett.* **52**, 997 (1984); K. Gross and W. Kohn, *ibid.* **55**, 2850 (1985).
- <sup>15</sup>M. Marques, C. A. Ullrich, F. Noguiera, A. Rubio, K. Burke, and E. K. U. Gross, eds., *Time-dependent Density Functional Theory* (Springer, Heidelberg, 2006).
- <sup>16</sup>E. Stenzel and H. Winter, *J. Phys. F* **15**, 1571 (1985).
- <sup>17</sup>S. Y. Savrasov, *Phys. Rev. Lett.* **81**, 2570 (1998).
- <sup>18</sup>J. B. Staunton, J. Poulter, B. Ginatempo, E. Bruno, and D. D. Johnson, *Phys. Rev. Lett.* **82**, 3340 (1999); *Phys. Rev. B* **62**, 1075 (2000).
- <sup>19</sup>P. Buczek, A. Ernst, and L. M. Sandratskii, *Phys. Rev. Lett.* **105**, 097205 (2010); P. Buczek, A. Ernst, P. Bruno, and L. M. Sandratskii, *ibid.* **102**, 247206 (2009); P. Buczek, Ph.D. thesis, Martin-Luther University, Halle-Wittenberg, 2009.
- <sup>20</sup>M. Niesert (unpublished).
- <sup>21</sup>S. Lounis, A. T. Costa, R. B. Muniz, and D. L. Mills, *Phys. Rev. Lett.* **105**, 187205 (2010).
- <sup>22</sup>F. Aryasetiawan and K. Karlsson, *Phys. Rev. B* **60**, 7419 (1999); K. Karlsson and F. Aryasetiawan, *ibid.* **62**, 3006 (2000); *J. Phys. Condens. Matter* **12**, 7617 (2000).
- <sup>23</sup>E. Sasioglu, A. Schindlmayr, C. Friedrich, F. Freimuth, and S. Blügel, *Phys. Rev. B* **81**, 054434 (2010).
- <sup>24</sup>R. D. Lowde and C. G. Windsor, *Adv. Phys.* **19**, 813 (1970).
- <sup>25</sup>F. J. Himpsel, *J. Magn. Magn. Mater.* **102**, 261 (1991).
- <sup>26</sup>N. Papanikolaou, R. Zeller, and P. H. Dederichs, *J. Phys. Condens. Matter* **14**, 2799 (2002).
- <sup>27</sup>A. I. Lichtenstein, M. I. Katsnelson, V. P. Antropov, and V. A. Gubanov, *J. Magn. Magn. Mater.* **67**, 65 (1987).
- <sup>28</sup>M. I. Katsnelson and A. I. Lichtenstein, *J. Phys. Condens. Matter* **16**, 7439 (2004).
- <sup>29</sup>K. Wildberger, P. Lang, R. Zeller, and P. H. Dederichs, *Phys. Rev. B* **52**, 11502 (1995).
- <sup>30</sup>O. K. Andersen, *Phys. Rev. B* **12**, 3060 (1975).
- <sup>31</sup>H. Krakauer, M. Posternak, and A. J. Freeman, *Phys. Rev. B* **19**, 1706 (1979); E. Wimmer, H. Krakauer, M. Weinert, and A. J. Freeman, *ibid.* **24**, 864 (1981).
- <sup>32</sup>D. L. Mills and P. Lederer, *Phys. Rev.* **160**, 590 (1967).
- <sup>33</sup>S. Lounis, Ph. Mavropoulos, P. H. Dederichs, and S. Blügel, *Phys. Rev. B* **72**, 224437 (2005); S. Lounis, Ph. Mavropoulos, R. Zeller, P. H. Dederichs, and S. Blügel, *ibid.* **75**, 174436 (2007); S. Lounis, M. Reif, Ph. Mavropoulos, L. Glaser, P. H. Dederichs, M. Martins, S. Blügel, and W. Wurth, *Europhys. Lett.* **81**, 47004 (2008); S. Lounis, P. H. Dederichs, and S. Blügel, *Phys. Rev. Lett.* **101**, 107204 (2008); S. Lounis and P. H. Dederichs, *Phys. Rev. B* **82**, 180404(R) (2010).
- <sup>34</sup>Ph. Mavropoulos, S. Lounis, and S. Blügel, *Phys. Status Solidi B* **247**, 1187 (2010); Ph. Mavropoulos, S. Lounis, R. Zeller, and S. Blügel, *Appl. Phys. A* **82**, 103 (2006).
- <sup>35</sup>O. Sipr, S. Bornemann, J. Minár, S. Polesya, V. Popescu, A. Simunek, and H. Ebert, *J. Phys. Condens. Matter* **19**, 096203 (2007).
- <sup>36</sup>A. Bergman, L. Nordstrom, A. B. Klautau, S. Frota-Pessoa, and O. Eriksson, *Phys. Rev. B* **73**, 174434 (2006); R. Robles and L. Nordstrom, *ibid.* **74**, 094403 (2006).
- <sup>37</sup>R. Vollner, M. Etzkom, P. Anil Kumar, H. Ibach, and J. R. Kirschner, *Phys. Rev. Lett.* **91**, 147201 (2003).